Wehrlite xenoliths and petrogenetic implications, Hosséré Do Guessa volcano, Adamawa plateau, Cameroon

Oumarou Faarouk Nkouandou, Jacques-Marie Bardintzeff, Zénab Nouraan Njankouo Ndassa, Aminatou Fagny Mefire, Adama Haman

Research Article

Oumarou Faarouk Nkouandou, Jacques-Marie Bardintzeff*,
Zénab Nouraan Njankouo Ndassa, Aminatou Fagny Mefire, and Adama Haman

Wehrlite xenoliths and petrogenetic implications, Hosséré Do Guessa volcano, Adamawa plateau, Cameroon

https://doi.org/10.1515/geo-2022-0408
received January 27, 2022; accepted September 15, 2022

Abstract: Peridotite xenoliths of wehrlite composition, scarcely known in Adamawa plateau, Cameroon, were sampled by Mio-Pliocene basanites from Hosséré Do Guessa volcano. Their origins are discussed and elucidated trough petrography and mineral chemistry. Studied wehrlites exhibit poikilitic or protogranular textures and are composed of four main mantle phases (high Mg-olivine, augite, enstatite and Al-spinel). Petrographic and microprobe (Camebax SX100) chemical data (Fo90.8-91.4 olivine, Wo39.4-42.0 augite, En90.5-91.1 enstatite and Al-spinel) suggest a mantle origin for the Hosséré Do Guessa wehrlites. Hence, these rocks could not be considered cumulate. They have been equilibrated between 1,140 and 1,220°C, at pressures of 1.5–2.0 GPa, at 50–66 km deep, below the crust-mantle boundary. Wehrlites might result in reactions with carbonate/carbonatite melt, accompanying CO_2 degassing and metasomatism by fluid phases. They suffered transpressional tectonics, during movement at Tertiary times of Pan-African strike-slip-faults, after solid-state tectonic relaxation.

Keywords: wehrlite, metasomatism, Hosséré Do Guessa, Adamawa plateau, Cameroon

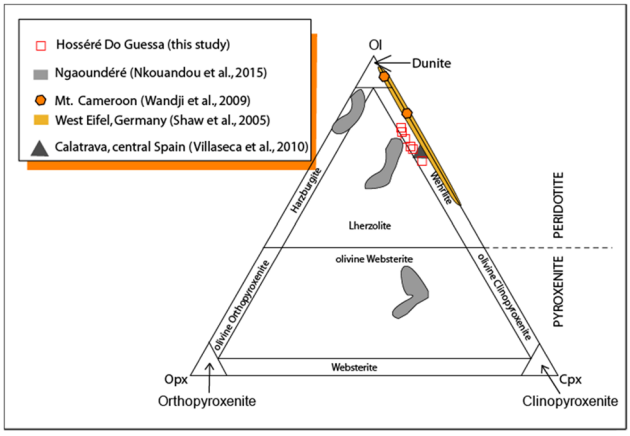

Graphical abstract

1 Introduction

The Cameroon Volcanic Line (CVL) is a Y-shaped oceanic and continental tectono-magmatic megastructure. Numerous volcanoes and plutonic-volcanic ring complexes, dated from Cenozoic to Quaternary compose the N30°E-trending CVL s.s. and the N70°E-trending Adamawa plateau, intersecting at Tchabal Mbabo volcano [1]. The internal structure of the Adamawa sub-continental mantle is still debated according to different studies.

Seismic and gravity studies [2–12] evidence (1) a crustal uplift resulting of the upward migration of the lithosphere-asthenosphere boundary, (2) an abnormally hot upwelling upper mantle located at the depth of 70–90 km [13] and (3) two broad negative gravity anomalies (–80 to –100 and –120 mGal/cm), attributable to lithospheric and crustal (crust is locally only 20 km thick) thinning.

Petrographical and mineral chemistry studies of numerous peridotite xenoliths found in the basaltic lavas evidence that they should be considered as fragments of the sub-continental lithosphere [14]. Ultramafic mantle xenoliths were sampled by Mio-Pliocene basanite lavas and pyroclastite projections on their

* **Corresponding author: Jacques-Marie Bardintzeff,** Univ Paris-Saclay, Department of Sciences de la Terre, Volcanologie-Planétologie, UMR CNRS 8148 GEOPS, bât. 504, F-91405 Orsay, France, e-mail: jacques-marie.bardintzeff@universite-paris-saclay.fr
Oumarou Faarouk Nkouandou: Department of Earth Sciences, Faculty of Sciences, University of Ngaoundéré, P.O. Box. 454, Ngaoundéré, Cameroon; Department of Mineral Engineering, Chemical Engineering and Minerals Industry School, University of Ngaoundéré, P.O. Box. 454, Ngaoundéré, Cameroon
Zénab Nouraan Njankouo Ndassa, Aminatou Fagny Mefire, Adama Haman: Department of Earth Sciences, Faculty of Sciences, University of Ngaoundéré, P.O. Box. 454, Ngaoundéré, Cameroon

way to the surface [3,15–18]. In the whole Adamawa plateau, ultramafic xenoliths display a compositionally diverse suite (spinel lherzolite, garnet lherzolite, olivine websterite, harzburgite). Mineral compositions, textures and thermobarometric conditions (820–1,160°C, 0.8–2.5 GPa, corresponding to different sampling depths of those rocks) evidence compositional heterogeneity of ~57-km-thick lithospheric mantle (from 26 to 83 km in depth) beneath the Adamawa plateau with limited asthenosphere uprise [17,18].

This article describes newly discovered wehrlite xenoliths. They occur in Hosséré Do Guessa volcano, close to Mazélé, in the northernmost region of Ngaoundéré. The study includes mineral chemistry of xenoliths compared to those of host rock and geothermobarometry.

2 Geological setting

Hosséré Do Guessa volcano is located within Adamawa plateau (AP), a south-trending asymmetrical horst limited by a cliff in its northern side. The asymmetry could result from the difference between the north, where the plateau is elevated on a rather thin 23 km crust and the south with a classical ~30–33 km crust [19]. The granulitic Pan-African (500–600 Ma) basement [20,21] is bounded to the north and to the south (Figure 1) by Pan-African N70° strike-slip faults [22,23]. These faults extend from Cameroon to Sudan along about 2,000 km [24] and crosscut the entire Adamawa lithosphere (crustal basement and upper mantle) down to depths greater than 190 km [6,13,19]. They have favored the ascent of alkaline magmas [22,25], which sampled fragments of sub-continental mantle xenoliths on their way to the surface. Geophysical studies carried out on the Adamawa plateau [6–12] show that a deflected and thin lithosphere with an effective elastic thickness of about 20 km [6]. Three major density contrasts were evidenced [6,19]: (1) the shallowest (4–15 km) boundary may be correlated to thrust structures and/or bottoms of sedimentary basins; (2) the 33–37 km boundary corresponds to the Moho; and (3) the 70–90 km boundary represents the lithosphere-asthenosphere boundary. From these different studies, a crust of 20–30 km thick and a lithosphere of 80–90 km thick seem to be evidenced in this region.

Previous petrologic studies on Adamawa mantle xenoliths [4,15–18,26] have shown that ultramafic xenoliths differ in nature and composition from each volcanic center to others. The present work is focused on the newly discovered ultramafic wehrlite xenoliths entrained by Mio-

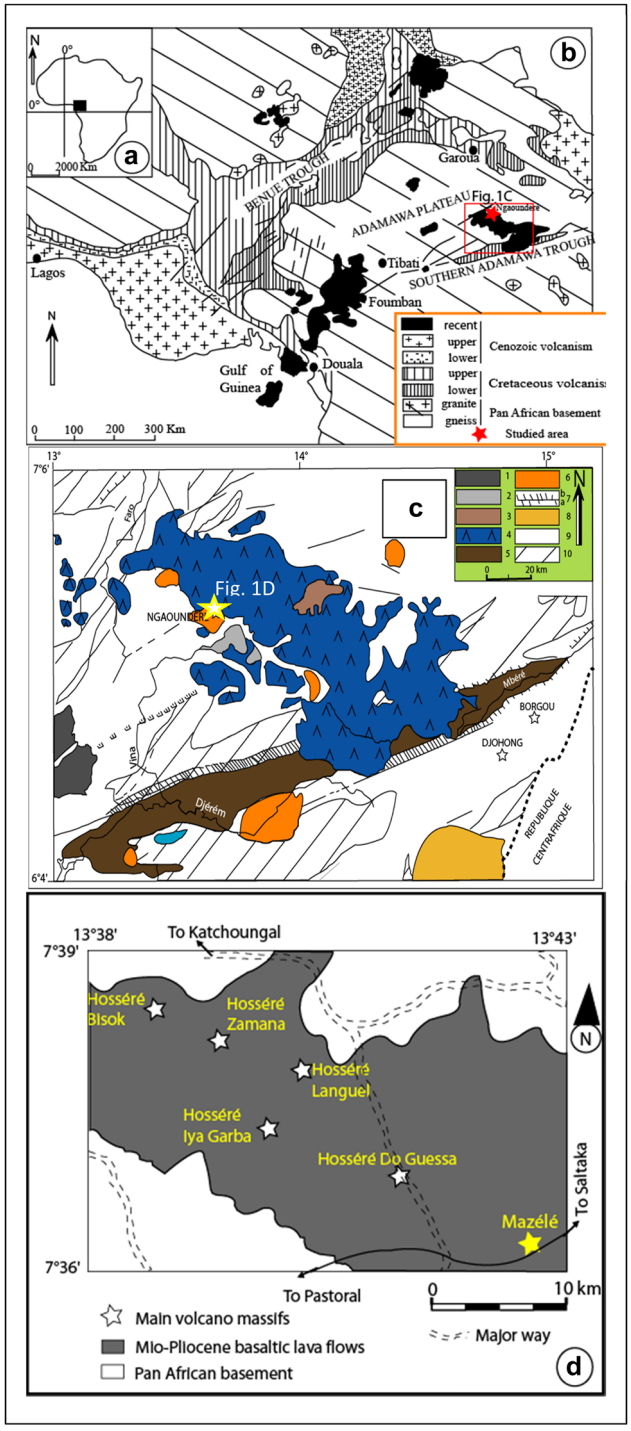

Figure 1: (a) Location of region of study in Africa continent, (b) main volcanic structures in Cameroon after [29]; red star shows the studied Hosséré Do Guessa volcano area in northern Ngaoundéré and (c) geological sketch map of Adamawa plateau (after [29]. (1) lateritic breastplate; (2) basalt of upper lava series; (3) trachyte and rhyolite; (4) basalt; (5) sedimentary rocks of southern Adamawa ditch, (a) metamorphic conglomerate and (b) conglomerate and arkose; (6) late panafricain granites; (7) schiste from Lom; (8) panafricain granites; (9) migmatite and gneiss; and (10) faults (a) with uprisde morphology and (b) with mylonite. (d) Location of Hosséré Do Guessa volcano near the village of Mazélé (yellow star).

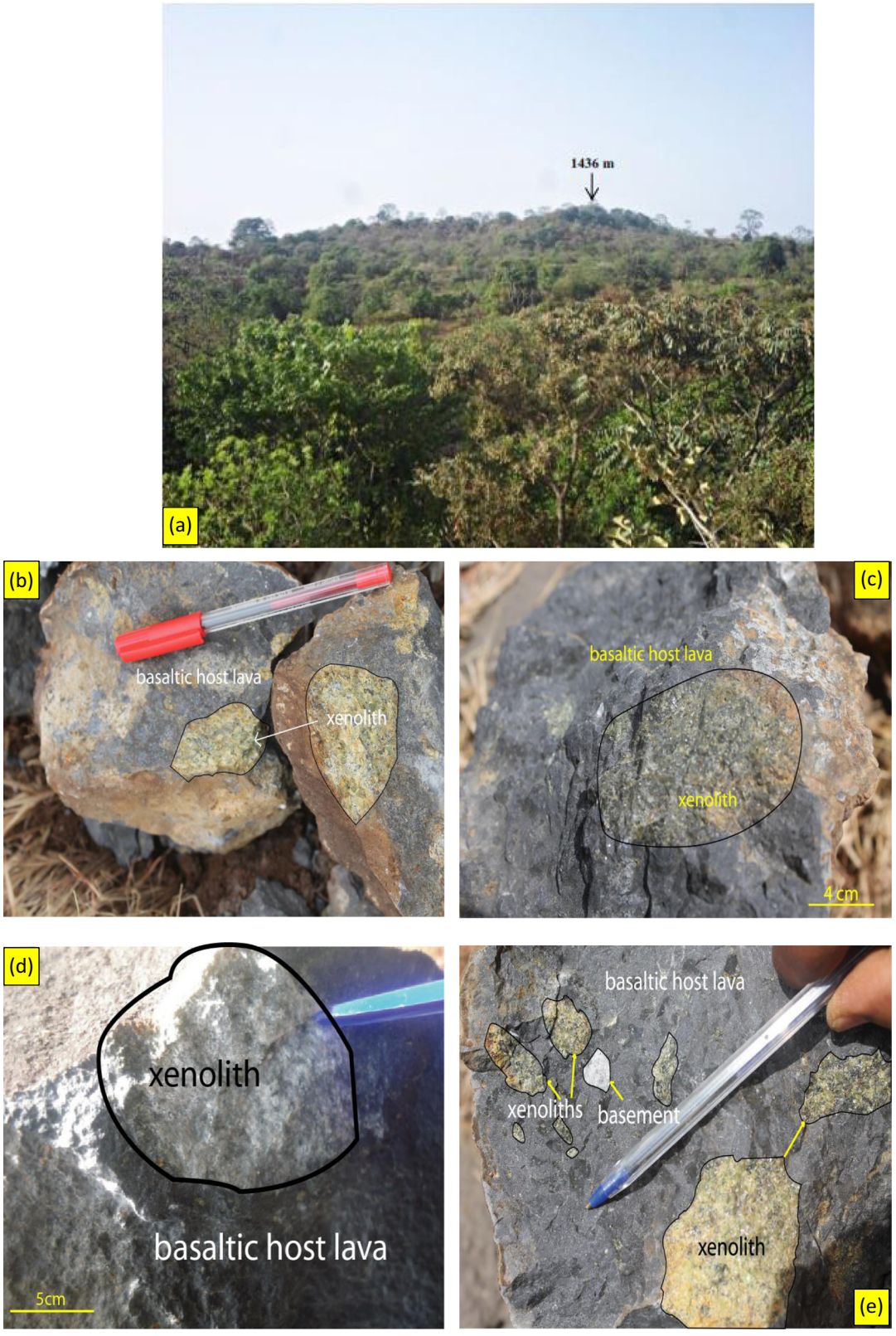

Figure 2: (a) View of the NE flank of Hosséré Do Guessa volcano. Peridotite xenoliths in host basanitic lava of Hosséré Do Guessa volcano. (b and c) rounded and (d and e) sub-angular shapes. Blue and red pens are 10 cm long.

Pliocene basaltic lavas along the Pan-African cracks at the northernmost edge of Adamawa plateau in Hosséré Do Guessa volcano. Wehrlites were only scarcely described in Adamawa plateau [26].

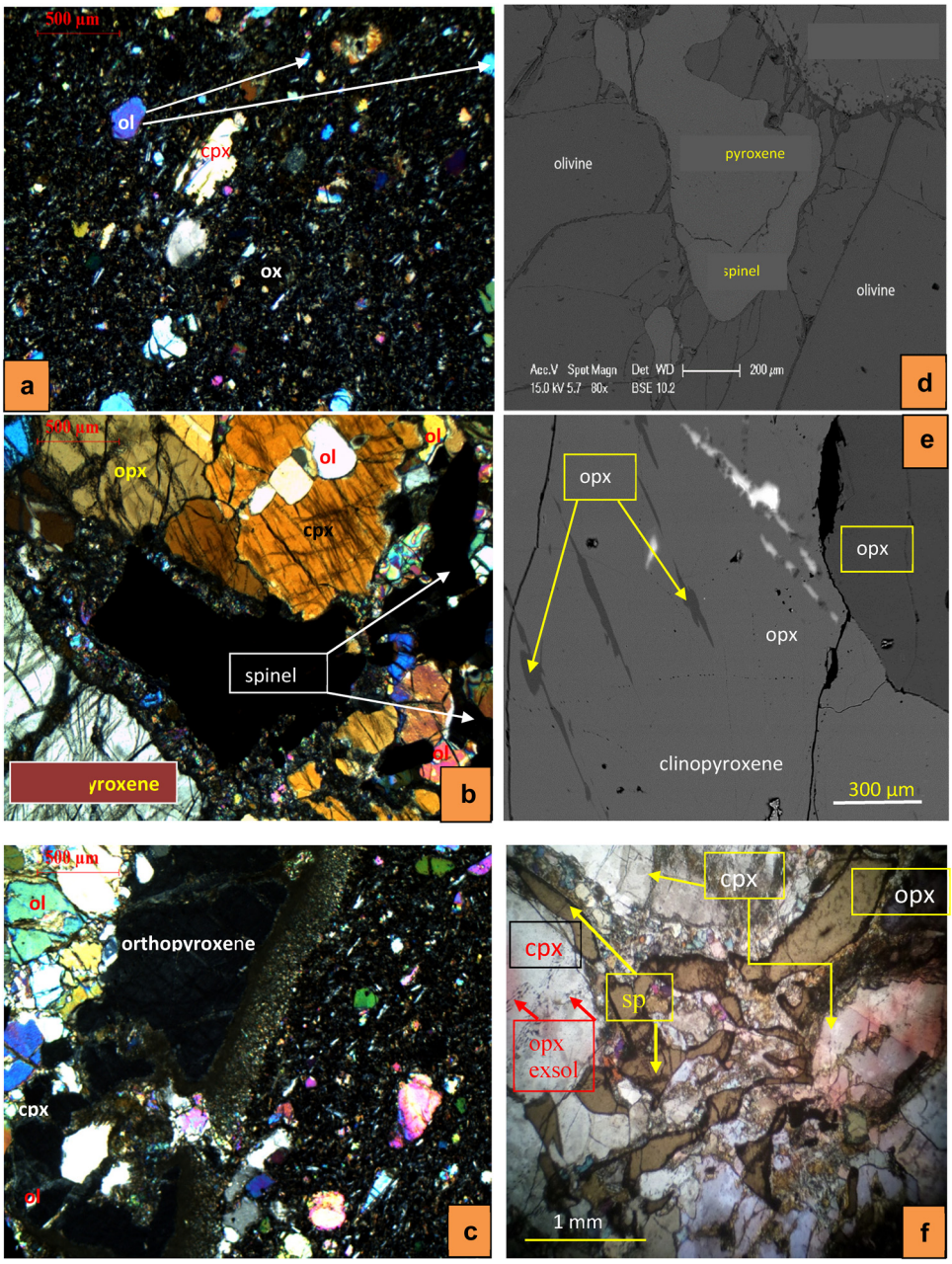

Figure 3: Photomicrographs of host basaltic lava (a) and xenoliths (b–e): wehrlite poikilitic texture (b and c), BSE images of representative peridotite samples showing: intimate contact between olivine and orthopyroxene (d), symplectite reaction with vermicular spinel between orthopyroxene crystals and exsolution (exsol) lamellas of orthopyroxene in clinopyroxene (e). cpx = clinopyroxene, ol = olivine, opx = orthopyroxene, sp = spinel.

3 Materials and methods

Petrographic studies have been carried out on about ten polished thin sections prepared from representative samples of ultramafic xenoliths at GEOPS laboratory, Université Paris-Saclay, France. Modal proportions of the four major mineral phases (olivine, orthopyroxene, clinopyroxene and spinel) have been estimated under scanning electron microscope (SEM), partly in Laboratory of Physics, University of Alexandru Ioan Cuza, Iasi, Romania, and partly in the GEOPS laboratory, Université Paris-Saclay, France.

Mineral compositions of host lavas and ultramafic xenoliths were analyzed on Camebax SX100 microprobe at Camparis, Université Paris-Sorbonne, France. The operating conditions were: olivine and clinopyroxene:

15 kV accelerating voltage and 40 nA beam current, 20 s counting time, except Si for olivine (10 s) and Ti for pyroxene (30 s); plagioclase: 15 kV, 10 nA, 10 s; titanomagnetite: 15 kV and 40 nA; Si, Ca, Ni: 10 s; Mn: 25 s; Cr: 15 s; Al: 30 s; and Ti, Fe, Mg: 40 s. Standards used were a combination of natural and synthetic minerals: diopside for Si, Ca and Mg; Fe_2O_3 for Fe; $MnTiO_3$ for Ti and Mn; Cr_2O_3 for Cr; albite for Na; and orthoclase for K and Al. Data corrections were made using the PAP correction [27].

4 Results

4.1 Field work and petrography

4.1.1 Hosséré Do Guessa volcano

The basement of Adamawa Plateau is cut by a Panafrican fault network. Small volcanic centers were emplaced at fault crossings. These are also fissural flows without noticeable crater.

Hosséré Do Guessa volcano is located at N07°37′32″ and E13°41′06″. It culminates at 1,436 m, 17 m above the surrounding floor and presents a low elevation of rather rectangular form of 350 m × 260 m, elongated along the SW–NE direction (Figure 2a). Volume of volcanites ranges between 1.0 and 1.5×10^6 m^3. Lava occur as dark grey loose blocks, which have a diameter of 1–1.5 m on the top of the hill and 20–50 cm in diameter on the flanks. They show a 1–3-mm-thick brown patina, and angular or rounded centimeter-size cavities (Figure 2b–e).

Basaltic host lava presents microlitic porphyritic texture (Figure 3a) that displays euhedral and subhedral olivine (15–18 vol%), clinopyroxene crystals (5–10 vol. %) sometimes with skeletal shape and oxides phenocrysts (<5 vol%). Plagioclase (20–25 vol%) and clinopyroxene (5 vol%) microliths are oriented along the flow foliation.

4.1.2 Peridotite xenoliths

Studied peridotite mantle xenoliths are collected in Mio-Pliocene basaltic lava flows of Hosséré Do Guessa volcano, 35 km at the northern edge of Ngaoundéré, near the so-called "Ngaoundéré cliff" (Figure 1b). The basement of this locality is delineated by numerous NW-SE shortening Pan-African faults [28,29], which may be related to the effect of the tectonic compression on the Adamawa plateau [29].

Yellowish, greenish and dark peridotite xenoliths have sizes of 8–15 cm and exhibit various shapes (angular, elongated or rounded shape, Figure 2). Contacts between xenoliths and host basaltic lavas are sharp (Figure 2c–e).

Modal compositions of xenoliths, estimated by microscopic observations and SEM images, are listed in Table 1. Their mineralogy is largely dominated by olivine (75–85%) and clinopyroxene (7–18%). The rest (5–8%) is composed of orthopyroxene and spinel.

According to the IUGS classification [30] (Figure 4), they are wehrlites, or lherzolites close to wehrlite-lherzolite boundary (samples TZ21 and TZ110). They present some similarities with wehrlites from Mt. Cameroon [31], West Eifel, Germany [32] and central Spain [33].

Textures are poikilitic (Figure 3b) or protogranular (Figure 3c–f) following [34], with some recrystallized olivine crystals.

Large (up to 7 mm) olivine crystals are weakly altered with thin micrometre-scale iddingsitized rims (Figure 3c).

Table 1: Sample location and modal mineral compositions (in volume%) of Hosséré Do Guessa wehrlites

Locality	Sample number	GPS coordinates	Olivine	Clinopyroxene	Orthopyroxene	Spinel
Mazélé	TZ13	N: 07° 37′31.4″ E: 13° 41′11.1″	76	16	4	4
Mazélé	NZ-B1	N: 07° 37′31.9″ E: 13° 41′07.2″	77	18	4	1
Mazélé	TZ21	N: 07° 38′23.9″ E: 13° 40′51.0″	79	13	5	3
Mazélé	BM1	N: 07° 38′22.7″ E: 13° 40′51.8″	79	13	4	4
Mazélé	TZ110	N: 07° 38′25.6″ E: 13° 40′47.8″	75	17	5	3
Mazélé	MZ11	N: 07° 38′22.53″ E: 13° 41′08.4″	85	7	4	4

Smaller (200 µm) light-colored olivine crystals are included within large clinopyroxene crystals (Figure 3b) and exhibit no indications of deformation, or alteration.

Clinopyroxene crystals are large (500 µm to 5 mm) and constitute the poikilitic phase enclosing small olivine crystals (Figure 3b). Orthopyroxene crystals are interlocked with olivine as shown trough Back-Scattered Electron (BSE) images (Figure 3d). Spinel occurs as intercrystalline dark crystals (50 µm to 3 mm) (Figure 3b) or surrounds clinopyroxene (Figure 3d). Elongated (10–100 µm, rarely up to 0.5 mm long) exsolution lamellae of orthopyroxene within clinopyroxene occur seldom (Figure 3f). Dark brown spinel crystals exhibit vermicular shape. Symplectite textures of clustered pyroxene and spinel are frequent (Figure 3f).

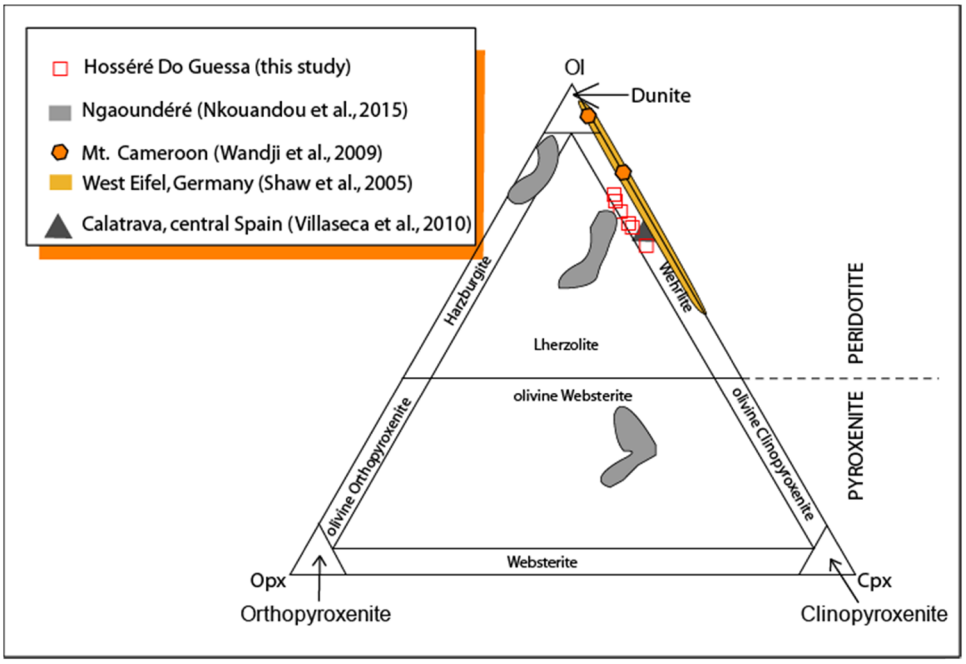

Figure 4: Ternary plot of olivine (Ol), orthopyroxene (Opx) and clinopyroxene (Cpx) modal compositions of the studied peridotite xenoliths after the IUGS nomenclature [30]. Data from Cameroon, Germany and Spain are added for comparison.

Table 2: Host lava (LTZ13) chemical composition and CIPW-normative composition calculated with $Fe_2O_3/FeO = 0.15$ [35,36]

LTZ13											
Major elements (wt%)											
SiO_2	TiO_2	Al_2O_3	Fe_2O_3	MnO	MgO	CaO	Na_2O	K_2O	P_2O_5	LOI	Sum
43.26	2.68	12.26	11.49	0.17	14.02	9.95	3.20	1.48	0.64	0.20	99.35
CIPW normative analysis (wt%)											
Or	Ab	An	Ne	Dio	Ol	Mt	Ilm	Apt			
8.75	4.58	14.72	12.18	24.41	24.95	1.98	5.09	1.48			
Trace elements (ppm)											
Be	Rb	Sr	Cs	Ba	V	Cr	Co	Ni	Cu	Y	Zr
2.0	38	759	0.40	538	220	65.0	59.7	382.8	38	22.5	237
Hf	Ta	Th	Nb	Zn	La	Ce	Pr	Nd	Sm	Eu	Gd
5.5	3.70	7.40	73	73	54.5	97	11.1	42	8.0	2.5	7.20
Tb	Dy	Ho	Tm	Yb	Lu						
0.980	5.04	0.91	0.28	1.80	0.24						

4.2 Whole rock and mineral chemistry

4.2.1 Host lava

The lava (sample LTZ13) host of xenolith sample TZ13 was studied in detail [35,36]. Its whole-rock chemical composition is listed in Table 2. It is a typical basanite, rather silica-poor (43.26 wt% SiO_2), but alkali rich ($Na_2O + K_2O$ = 4.68 wt%, Ba = 538 ppm), with CIPW-normative nepheline (12.18 wt%). Its rather primitive character is shown by high Ni content (383 ppm). Data of mineral chemistry were previously published [35,36]. Additional data are listed in Table 3.

Olivine phenocrysts have Fo71-79, decreasing from cores to rims and from phenocrysts to microcrysts, while olivine xenocrysts have high Fo contents (Fo88-90). CaO contents of olivine phenocrysts of host lava are high (0.25–0.55 wt% CaO) compared to low contents (0.10–0.15 wt%) in olivine xenocrysts. NiO contents of olivine phenocrysts are low (<0.2 wt%) whereas those of xenocrysts are higher (0.37–0.40 wt%).

Table 3: Representative microprobe compositions of major rock-forming minerals of Hosséré Do Guessa wehrlites host lava

Sample	**LTZ13**													
Mineral	**Olivine**									**cpx**	**pl**		**mt**	
Type	**Phenocryst**						**Xenocryst**			**Phenocryst**				
SiO_2 (wt%)	38.37	36.48	36.51	37.08	36.33	36.65	39.89	40.49	39.89	41.94	52.93	51.97	0.08	0.69
TiO_2										5.12			21.89	21.79
Al_2O_3										9.32	29.04	29.42	1.75	1.58
Cr_2O_3										0.04			0.12	0.17
FeO	19.42	24.68	23.65	24.04	24.36	22.84	10.13	9.55	11.94	4.90	0.86	0.89	67.79	65.01
Fe_2O_3										4.54				
MnO	0.40	0.48	0.54	0.52	0.60	0.42	0.15	0.12	0.21	0.11			0.90	1.03
MgO	40.04	37.10	37.44	37.62	36.66	38.71	49.66	49.41	47.31	10.54			3.54	3.41
NiO	0.23	0.14	0.09	0.24	0.13	0.19	0.40	0.37	0.40				0.00	0.00
CaO	0.25	0.49	0.46	0.49	0.45	0.30	0.10	0.12	0.15	22.14	11.27	12.03	0.07	0.70
Na_2O										0.56	4.55	4.47		
K_2O											0.41	0.19		
Sum	98.71	99.37	98.69	99.99	98.53	99.11	100.33	100.06	99.90	99.21	99.06	98.97	96.14	94.38
Si (apfu)	0.999	0.965	0.968	0.972	0.969	0.962	0.973	0.990	0.989	6.395	2.418	2.384	0.024	0.206
Ti										0.587			4.813	4.872
Al^{IV}										1.605				
Al^{VI}										0.070				
Cr										0.005			0.029	0.040
Fe^{3+}										0.521			5.527	5.081
Fe^{2+}	0.423	0.546	0.524	0.527	0.544	0.502	0.207	0.195	0.248	0.624	0.033	0.034	11.047	11.082
Mn	0.005	0.011	0.012	0.011	0.014	0.009	0.003	0.002	0.004	0.014			0.224	0.259
Mg	1.554	1.462	1.480	1.470	1.458	1.515	1.806	1.801	1.747	2.395			1.545	1.513
Ni	0.009	0.003	0.002	0.005	0.003	0.004	0.008	0.007	0.008					
Ca	0.007	0.014	0.013	0.014	0.013	0.009	0.003	0.003	0.004	3.617	0.552	0.591	0.022	0.224
Na										0.166	0.403	0.397		
K											0.024	0.011		
Mg#	78.61	72.81	73.85	73.61	72.83	75.11	89.72	90.23	87.57	67.65				
% Usp													61.49	64.51
Wo										50.44				
En										33.40				
Fs										16.17				
An											56.30	59.12		
Ab											41.26	39.77		
Or											2.44	1.11		

Structural formulas: olivine on the basis of 4 oxygen anions, clinopyroxene on the basis of 16 cations, plagioclase on the basis of 8 oxygen anions, Ti-magnetite on the basis of 32 oxygen anions.

Clinopyroxene phenocrysts are augite and diopside (Wo 43.2–48.4), some with fassaitic composition (Wo 50.4) as those described in Noun Plain, Cameroon [37]. TiO_2 contents (2.7–5.1 wt%) and Al_2O_3 contents (from 6.6 to 9.3, until 12.4 wt%) are high. Mg# ratios (68–76) are in the range as olivine.

Oxide phenocrysts and microcrysts are Ti-magnetite (TiO_2: 21.8–21.9 wt% and FeOt: 65.0–67.8 wt%). Cr_2O_3 contents are low (0.12–0.17 wt%), while MgO contents are fairly constant (3.4–3.5 wt%).

4.2.2 Wehrlite xenoliths

Representative microprobe analyses of olivine, orthopyroxene, clinopyroxene and spinel are listed in Tables 4–6.

Olivine varies in Fo between 90.8 and 91.4 (Table 4) and CaO contents are very low (<0.1 wt%). High NiO contents range between 0.24 and 0.48 wt%.

Clinopyroxene (Table 5) is augite (Figure 5) with Wo39.4–42.0 En48.5–51.2 Fs9.0–9.6. TiO_2 (0.76–1.27 wt%) contents are fairly low and Al_2O_3 (5.00–5.88 wt%) contents are high. Cr_2O_3, contents range between 0.89 and 0.99 wt%. Na_2O contents between 0.68 and 1.18 wt% are somewhat high for mantle pyroxene. Mg# (=Mg/Mg + Fe) are fairly constant, between 84.2 and 85.8. In TiO_2 (wt%) in pyroxene versus Mg# in coexisting olivine diagram (Figure 6, according to [38]), wehrlite minerals plot higher than the lherzolite field. In the MgO versus Al_2O_3 diagram (Figure 7, after [39]), clinopyroxene compositions plot within the spinel peridotite field.

Orthopyroxene (Table 5) is enstatite (after [40]) with Wo0.8–1.0 En90.5–91.1 Fs7.9–8.6. Al_2O_3 contents (0.72–1.28 wt%) are low and fairly constant whereas Cr_2O_3 contents (0.02–0.05 wt%) are very low. Mg# ratios (91.7–92.2) are higher than in clinopyroxene and slightly higher than in olivine.

Spinel (Table 6) is Al-spinel after [41]. It shows some contrasted compositions, with varying Cr# (11.9–27.3) and Fe^{3+}# (5.3–10.7). In Fo versus Cr# OSMA diagram (after [42], Figure 8), wehrlites plot in the mantle spinel array.

4.3 Thermobarometry

Equilibrium temperatures, pressures and depths of wehrlite from Hosséré Do Guessa volcano have been estimated through several currently available and appropriate thermobarometers based on different exchange mechanisms (Table 7, Figure 9). Crystal core compositions have been preferentially used for calculations.

4.3.1 Host lava

Tentative calculations were based on olivine – liquid/glass [43] and clinopyroxene – liquid/glass [44] geothermometers.

Table 4: Representative microprobe compositions of olivine of Hosséré Do Guessa wehrlite and structural formulas on the basis of 4 oxygen anions

Sample	TZ13													
n0	1	2	3	4	5	6	7	8	9	10	11	12	13	14
SiO_2 (wt%)	41.16	41.12	40.77	40.36	40.77	40.81	40.63	40.92	40.78	40.87	40.66	41.12	40.61	40.78
FeO	8.52	8.39	8.52	8.86	8.80	8.70	8.76	8.73	8.35	8.68	8.75	8.51	8.64	8.86
MnO	0.20	0.11	0.14	0.14	0.06	0.16	0.19	0.18	0.17	0.20	0.18	0.17	0.12	0.17
MgO	50.51	50.32	50.75	50.28	50.46	50.15	50.15	50.11	50.13	50.32	50.61	50.36	50.44	50.30
CaO	0.03	0.03	0.04	0.06	0.05	0.02	0.05	0.08	0.03	0.04	0.06	0.06	0.06	0.03
NiO	0.36	0.48	0.43	0.44	0.37	0.24	0.42	0.46	0.45	0.34	0.36	0.36	0.37	0.41
Sum	100.78	100.45	100.65	100.14	100.51	100.08	100.20	100.48	99.91	100.45	100.62	100.58	100.24	100.55
Si (apfu)	0.996	0.998	0.989	0.987	0.991	0.995	0.991	0.995	0.996	0.994	0.988	0.997	0.990	0.992
Fe^{2+}	0.172	0.170	0.173	0.181	0.179	0.177	0.179	0.177	0.171	0.176	0.178	0.173	0.176	0.180
Mn	0.004	0.002	0.003	0.003	0.001	0.003	0.004	0.004	0.003	0.004	0.004	0.003	0.002	0.003
Mg	1.823	1.821	1.836	1.832	1.829	1.823	1.824	1.817	1.825	1.824	1.834	1.821	1.833	1.824
Ca	0.001	0.001	0.001	0.001	0.001	0.000	0.001	0.002	0.001	0.001	0.002	0.001	0.002	0.001
Ni	0.007	0.009	0.008	0.009	0.007	0.005	0.008	0.009	0.009	0.007	0.007	0.007	0.007	0.008
Fo%	91.17	91.35	91.26	90.88	91.03	90.98	90.90	90.93	91.29	91.00	91.00	91.18	91.12	90.85

Table 5: Representative microprobe compositions of clinopyroxene and orthopyroxene of Hosséré Do Guessa wehrlite and structural formulas on the basis of 16 cations

Sample	TZ13											
Mineral	Clinopyroxene											
n0	1	2	3	4	5	6	7	8	9	10	11	12
SiO_2 (wt%)	50.79	51.19	51.16	50.82	51.06	51.89	51.44	51.62	50.77	51.77	52.15	50.70
TiO_2	0.96	0.86	0.87	0.84	0.77	0.76	0.85	0.83	1.27	0.81	0.82	0.75
Al_2O_3	5.88	5.66	5.45	5.41	5.37	5.51	5.44	5.43	5.00	5.33	5.40	5.51
Cr_2O_3	0.95	0.98	0.90	0.98	0.95	0.95	0.90	0.99	0.89	0.94	0.94	0.94
FeO*	4.04	4.71	4.34	3.52	2.93	4.09	4.31	3.88	4.33	3.92	4.62	0.02
Fe_2O_3*	1.57	0.84	0.90	2.00	2.77	1.22	1.09	1.60	1.24	1.02	0.55	5.41
MnO	0.04	0.16	0.10	0.16	0.09	0.11	0.08	0.13	0.23	0.10	0.12	0.08
MgO	16.29	16.47	16.34	16.73	16.62	16.87	16.24	16.50	16.27	16.39	16.55	16.80
NiO												0.16
CaO	18.47	18.34	18.29	17.93	18.45	18.42	18.79	18.73	19.62	19.26	18.80	18.89
Na_2O	1.04	0.92	1.07	1.09	1.18	1.05	1.05	1.09	0.68	1.02	1.03	1.06
Sum	100.03	100.13	99.42	99.48	100.19	100.87	100.19	100.80	100.30	100.56	100.98	100.32
Si (apfu)	7.396	7.448	7.485	7.429	7.416	7.477	7.478	7.457	7.407	7.491	7.513	7.311
Ti	0.105	0.094	0.096	0.092	0.084	0.082	0.093	0.090	0.139	0.088	0.089	0.082
A^{IIV}	0.604	0.552	0.515	0.571	0.584	0.523	0.522	0.543	0.593	0.509	0.487	0.689
Al^{VI}	0.406	0.419	0.424	0.362	0.336	0.412	0.410	0.382	0.267	0.401	0.430	0.247
Cr	0.109	0.113	0.104	0.113	0.109	0.108	0.103	0.113	0.103	0.107	0.107	0.108
Fe^{3+}	0.172	0.092	0.099	0.220	0.303	0.132	0.119	0.174	0.136	0.111	0.059	0.587
Fe^{2+}	0.492	0.573	0.531	0.430	0.356	0.492	0.524	0.469	0.529	0.474	0.556	0.002
Mn	0.005	0.020	0.012	0.020	0.011	0.013	0.010	0.016	0.028	0.012	0.015	0.010
Mg	3.535	3.571	3.563	3.645	3.598	3.623	3.518	3.552	3.538	3.535	3.554	3.611
Ni												0.019
Ca	2.882	2.859	2.867	2.809	2.871	2.844	2.927	2.899	3.067	2.986	2.902	2.919
Na	0.294	0.260	0.304	0.309	0.332	0.293	0.296	0.305	0.192	0.286	0.288	0.297
Mg#	84.19	84.31	84.97	84.86	84.53	85.30	84.55	84.68	84.18	85.81	85.23	85.96
Wo	40.67	40.19	40.54	39.43	40.22	40.03	41.23	40.78	42.03	41.96	40.96	40.94
En	49.89	50.20	50.37	51.17	50.40	50.99	49.57	49.96	48.47	49.66	50.15	50.65
Fs	9.44	9.62	9.08	9.41	9.38	8.98	9.20	9.26	9.50	8.38	8.90	8.41

Sample	TZ13							
Mineral	Orthopyroxene							
n0	13	14	15	16	17	18	19	20
SiO_2 (wt%)	57.74	58.00	57.73	57.89	58.17	57.92	53.41	54.41
TiO_2	0.00	0.00	0.00	0.00	0.00	0.00	0.30	0.32
Al_2O_3	1.28	0.76	0.84	0.84	0.72	0.74	4.58	4.37
Cr_2O_3	0.04	0.02	0.04	0.03	0.04	0.05	0.73	0.75
FeO*	5.27	5.22	5.08	4.09	5.12	5.06	4.84	6.49
Fe_2O_3*	0.45	0.14	0.32	1.45	0.53	0.57	4.01	1.98
MnO	0.29	0.19	0.19	0.18	0.12	0.11	0.13	0.09
MgO	35.11	35.39	35.31	35.90	35.67	35.47	30.70	30.59
NiO							0.10	
CaO	0.46	0.50	0.47	0.54	0.51	0.47	1.45	1.38
Na_2O	0.07	0.05	0.05	0.06	0.02	0.06	0.11	0.11
Sum	100.71	100.27	100.03	100.98	100.90	100.45	100.36	100.49
Si (apfu)	7.881	7.937	7.920	7.865	7.916	7.916	7.417	7.538
Ti	0.000	0.000	0.000	0.000	0.000	0.000	0.031	0.033
A^{IIV}	0.119	0.063	0.080	0.135	0.084	0.084	0.583	0.462
Al^{VI}	0.087	0.059	0.056	0.000	0.031	0.035	0.166	0.251
Cr	0.004	0.002	0.004	0.003	0.004	0.005	0.080	0.082
Fe^{3+}	0.046	0.015	0.033	0.148	0.054	0.059	0.419	0.206

(*Continued*)

Table 5: *Continued*

Sample	TZ13							
Mineral	Orthopyroxene							
n0	13	14	15	16	17	18	19	20
Fe^{2+}	0.601	0.598	0.583	0.465	0.583	0.578	0.563	0.752
Mn	0.034	0.022	0.022	0.021	0.014	0.013	0.015	0.011
Mg	7.142	7.217	7.219	7.269	7.234	7.225	6.354	6.316
Ni							0.012	0.000
Ca	0.067	0.073	0.069	0.079	0.074	0.069	0.216	0.205
Na	0.019	0.013	0.013	0.016	0.005	0.016	0.030	0.029
Mg#	91.69	92.18	92.14	92.22	91.90	91.90	86.62	86.82
Wo	0.85	0.93	0.87	0.98	0.93	0.87	2.86	2.74
En	90.52	91.07	91.08	91.07	90.88	90.96	83.97	84.31
Fs	8.63	8.00	8.05	7.95	8.18	8.18	13.17	12.94

FeO* and Fe_2O_3* recalculated according to a total of 16 cations.

However, calculated K_D are respectively 0.658 for olivine Fo 78.6, 0.902 for olivine Fo 72.8 and 0.960 for olivine Fo 71.1, that differ from the experimental equilibrium K_D of 0.300. Similarly, K_D are 0.715 for clinopyroxene Wo 50.4, 0.661 for Wo 48.4 and 0.850 for Wo 43.2, that differ from the experimental equilibrium K_D of 0.275. Actually, the basanite sample LTZ13 corresponds to a partly cumulative lava ("ankaramite" facies), containing also olivine xenocrysts (Table 3). Considering an assumed liquid (MgO = 8–9 wt%, FeO = 14–15 wt%) in equilibrium with olivine and pyroxene, temperature of 1,300°C and pressure of 11 kbar (1.1 GPa) are estimated.

4.3.2 Xenoliths

4.3.2.1 Thermometry

Graphical estimations in quadrilateral pyroxene diagram according to [45] suggest a temperature range from 920 to 1,080°C for a pressure of 5 kbar (0.5 GPa) (Figure 5) but note that these thermometric limits are nearly the same between 1 atm and 10 kbar.

More precise equilibrium temperatures of xenolith were determined by applying (1) the empirical single pyroxene thermobarometer of [46] based on Cr–Al solubility in (ortho- or clino-) pyroxene, (2) the two-pyroxenes thermometer of [47], based on Ca-exchange between clino- and ortho- pyroxenes, (3) the partitioning of Na between ortho- and clinopyroxenes and Ca (apfu) content of orthopyroxene alone proposed by [48], (4) olivine-spinel exchange of [49] and (5) clino-ortho-pyroxenes equilibrium of ref. [50]. For these calculations, only data on well crystallized and identified phases have been used to avoid any unknown mantle process which may occur during recrystallization process. Calculated temperatures are listed in Table 7.

Calculated temperatures using single pyroxene thermometer of [46] yield values between 840 and 900°C with orthopyroxene data, except two values at 1,260°C

Table 6: Representative microprobe compositions of spinel and structural formula on the basis of 24 total cations

Sample	TZ13		
Mineral	Spinel		
n0	1	11	13
SiO_2 (wt%)	0.92	0.25	0.21
TiO_2	0.91	1.77	1.28
Al_2O_3	50.51	37.89	44.07
Cr_2O_3	10.15	21.17	15.49
FeOt	18.94	18.08	22.15
MgO	17.70	19.65	17.01
NiO	0.35	0.46	0.22
CaO	0.02	0.01	0.08
Na_2O	0.03	0.01	0.01
Sum	99.53	99.29	100.52
Si (apfu)	0.197	0.055	0.046
Ti	0.147	0.296	0.211
Al^t	12.786	9.947	11.397
Cr	1.724	3.728	2.687
Fe^{3+}	0.812	1.629	1.406
Fe^{2+}	2.590	1.738	2.658
Mg	5.667	6.525	5.565
Ni	0.061	0.082	0.039
Ca	0.005	0.003	0.018
Na	0.010	0.005	0.003
Mg#	68.63	78.96	67.67
Cr#	11.88	27.26	19.08
Fe^{3+}#	5.30	10.65	9.08

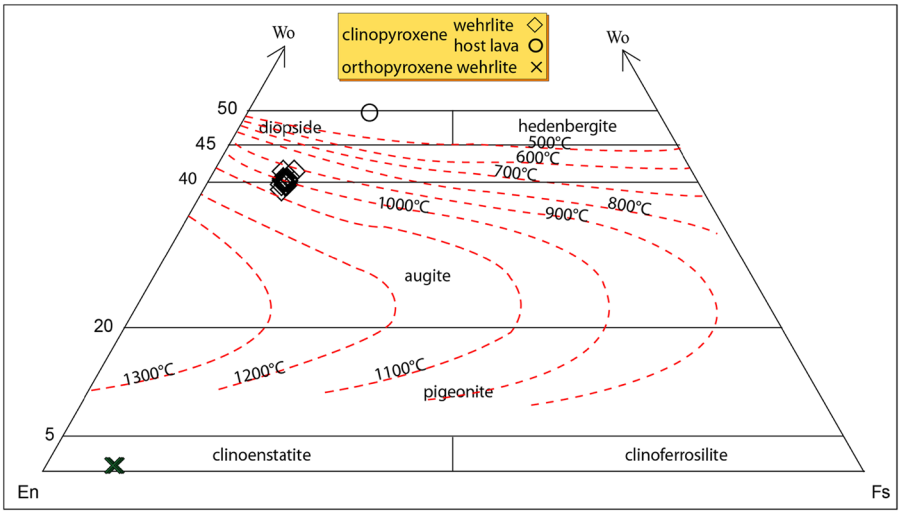

Figure 5: Pyroxene composition of Hosséré Do Guessa wehrlites and host lava in quadrilateral diagram after [40]. Thermometry between 500°C and 1,300°C according to [45] for P = 5 kbar (0.5 GPa).

(for orthopyroxene analyses 19 and 20 which are Cr-richer that witness deeper equilibrium) while values obtained when using clinopyroxene data are between 1,090 and 1,220°C (Table 7, Figure 9). Empirical two pyroxene method of [47] give the temperature values of 1,070–1,130°C while the range of 750–900°C (except 1,190°C for 19 and 20) have been obtained through formulae of [48] when using Na and Ca of pyroxene porphyrocrysts. Olivine-spinel exchange method of [49] give the temperature values of 1,005–1,220°C. Two-pyroxenes geothermometer of [50] was used. We obtain 1,183.4°C for cpx Ca-poorest versus opx Ca-poorest and 1,124.5°C for cpx Ca-richest versus opx Ca-poorest. Values with Cr-orthopyroxene 19 and 20 are up to 1,135°C.

Results are scattered. Values obtained with three thermometers (two single orthopyroxene and one cpx–opx of [46] and [48] are rather low (750–900°C). They do not likely correspond to wehrlite crystallization but reflect probably late re-equilibration. Values obtained with the single clinopyroxene [46], olivine–spinel [49] and cpx–opx [50] give higher temperatures (1,005–1,220°C), reflecting more probably crystallization temperatures of mantle xenoliths (see discussions in [48,51,52]. The same value of 1,180°C is

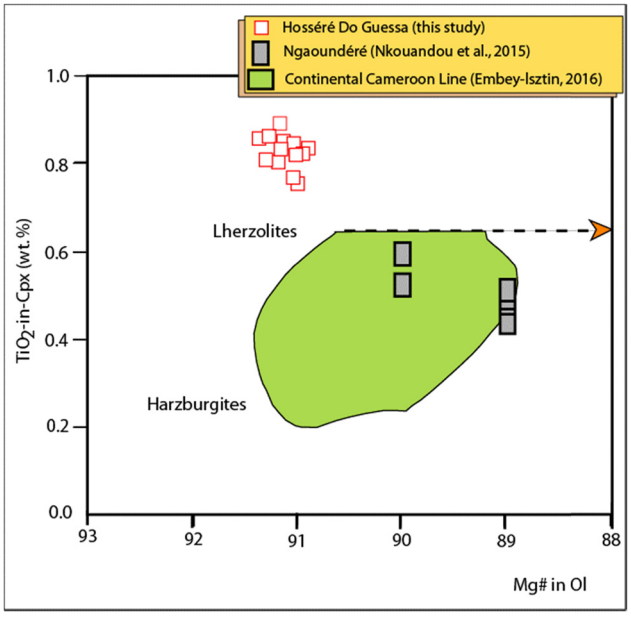

Figure 6: Mg# in Ol versus TiO_2 in Cpx in Hosséré Do Guessa wehrlite following [38]. Dashed line with arrow indicates the mantle refertilization.

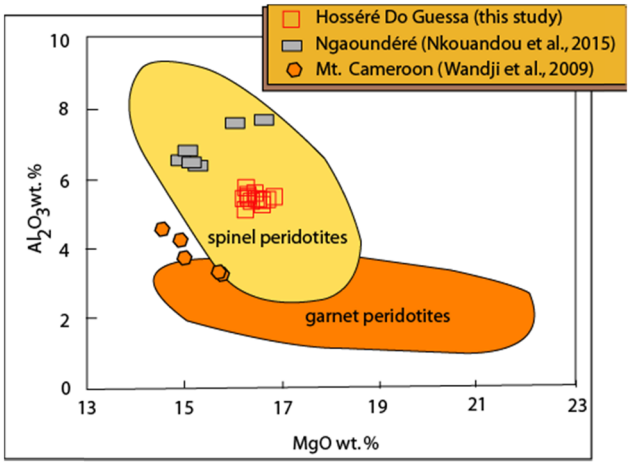

Figure 7: MgO versus Al_2O_3 for clinopyroxene of Hosséré Do Guessa wehrlites compared with other peridotites of Cameroon, plotted in the fields defined by ref. [39].

obtained with cpx Ca-poorest versus opx Ca-poorest thermometry of [50] and corresponds to the highest result with olivine-spinel thermometry. A bracket of 1,180 ± 40 = 1,140–1,220°C (maximum calculated) might match the effective temperature.

4.3.2.2 Barometry

Unfortunately, there is no direct method for determining equilibrium pressure in spinel peridotite xenoliths. Despite use of the Ca-in-olivine barometer [53] in some investigations, it has been demonstrated that it is incorrect, and its application may not provide reliable results [52,54,55].

Using formulas of [46], values from clinopyroxene mainly range from 0.58 to 0.94 GPa (and some values from 3.0 to 3.5 GPa corresponding to very deep pressures) whereas, from orthopyroxene, two groups of values are identified, one around 0.16 GPa and the second from 2.24 to 2.58 GPa (Table 7, Figure 9).

The two-pyroxenes geobarometer [50] give values between 1.4 and 2.1 GPa. In addition, assuming a temperature of 1,150°C, clinopyroxene yields pressures of 1.08–1.68 GPa (barometer of [56]). Several values, between 1.5 and 2.0 GPa, seem possible pressures of xenoliths formation. These values are close of those experimental equilibria (1.61–1.87 GPa) between spinel lherzolite and garnet lherzolite determined by [57]. Later, xenoliths have been reequilibrated from 0.9 to 0.6 GPa and possibly down to 0.16 GPa.

The corresponding depths using the conversion of 33 km/GPa are between 49.5 km (for 1.5 GPa) and 66 km (for 2.0 GPa), that is to say 33–37 km of crust plus 17–29 km of mantle.

When plotted in P-T diagram (Figure 9, adapted from [58]), calculated values form four clusters. The group with temperatures close to 1,100–1,200°C and pressures around 1.5–2.0 GPa obtained following [50] follow the same geotherm as the Youkou spinel lherzolite, in Adamawa, proposed by [58]. It corresponds to a fairly hot geotherm of 60 mW/m^2, between the "continental geotherm" and the "static rift geotherm." It is consistent with geophysical data obtained in Adamawa. Such high geotherm might result from the regional active tectonic and/or the occurrence of a rising mantle plume, as discussed by [59] for Ethiopian plateau.

5 Discussion

5.1 Mantle origin of Hosséré Do Guessa wehrlite xenoliths

Mio-Pliocene basanite lava flows and volcanic deposits in the Adamawa plateau [36,60,61] are characterized by the occurrence of a large number of ultramafic xenoliths [17,18,58]. Wehrlite xenoliths, discovered in Hosséré Do Guessa volcano, were unknown so far in the Adamawa Plateau.

These wehrlites exhibit poikilitic textures, which are sometimes ascribed to cumulate rocks crystalized from

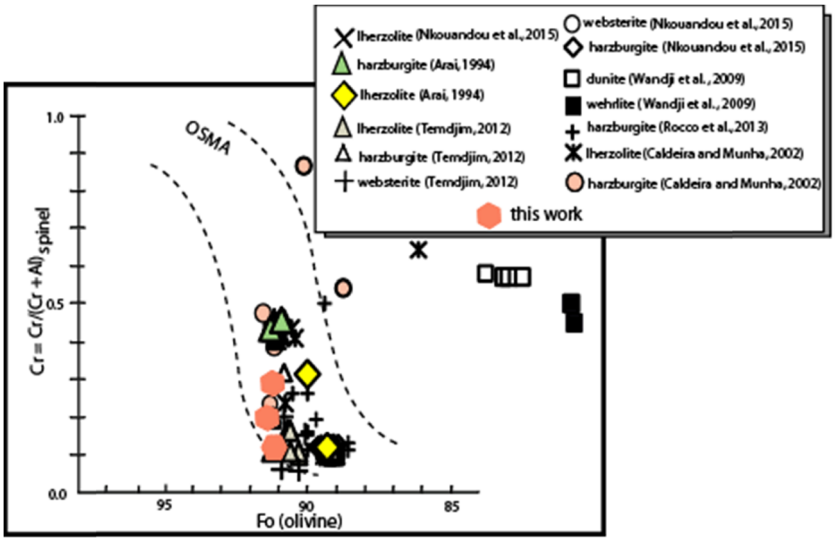

Figure 8: Fo (olivine) versus Cr# (spinel) diagram (after [42]). OSMA = olivine spinel mantle array. Data for peridotite xenoliths from Cameroon [18,31,75], São Tomé [76], Madagascar [77] and elsewhere in the world [42] are added for comparison.

Table 7: Temperature, pressure and depth estimations for Hosséré Do Guessa wehrlite

Sample/ method	TMOpx (°C) (n0 Opx)	TMCpx (°C) (n0Cpx)	TWOpx/Cpx (°C) (n0Cpx-n0-Opx)	TBKNaOpx/Cpx (°C) (n0Cpx-n0-Opx)	TBKCaOpx (°C) (n0Opx)	TOWOl/Sp (°C) (n0Ol-n0Sp)	TPCpx-Opx (°C) (n0Cpx-n0-Opx)
TZ13	899.9 (13)	1090.2 (1)	1091.0 (1–13)	754.6 (4–13)	751.8 (13)	1135.0 (1–1)	1172.0 (2–13)
TZ13	872.9 (14)	1219.2 (2)	1072.0 (2–13)	799.66 (5–13)	766.2 (14)	1137.0 (2–1)	1183.4 (4–13)
TZ13	874.2 (15)	1209.8 (3)	1092.0 (2–14)	767.2 (6–14)	756.1 (15)	1005.0 (3–1)	1124.5 (9–13)
TZ13	871.0 (16)	1183.1 (4)	1116.0 (4–14)	812.1 (7–16)	779.2 (16)	1152.0 (4–1)	1179.6 (4–16)
TZ13	850.2 (17)	1184.0 (5)	1100.0 (3–15)	802.4 (9–17)	768.7 (17)	1178.0 (5–1)	1125.2 (9–16)
TZ13	840.5 (18)	1189.0 (6)	1109.0 (5–15)	900.8 (10–18)	756.9 (18)	1160.0 (7–1)	1133.9 (12–19)
TZ13	1263.20 (19)	1154.5 (7)	1102.0 (6–16)	1194.8 (12–19)	1146.5 (20)	1087.0 (9–1)	1135.7 (12–20)
TZ13	1258.73 (20)	1162.2 (8)	1087.0 (1–17)	1191.2 (12–20)	1161.7 (19)	1089.0 (11–1)	
TZ13		1176.63 (9)	1131 (12–19)			1178.0 (6–11)	
TZ13		1210.65 (10)	1120 (12–20)			1223.2 (11–11)	
TZ13		1180.49 (11)				1177.7 (6–13)	
TZ13		1215.15 (12)				1197.9 (11–13)	
	PMOpx (GPa)/ Depth (Km)	PMCpx (GPa)/ Depth (Km)					PPCpx-Opx (GPa)/ Depth (Km)
TZ13	0.16 (13)/5.28	0.58 (1)/19.14					2.02 (2–13)/66.66
TZ13	2.24 (14)/73.94	0.71 (2)/23.43					2.10 (4–13)/69.30
TZ13	2.50 (15)/82.50	0.90 (3)/29.80					1.65 (9–13)/54.45
TZ13	2.43 (16)/80.32	0.94 (4)/31.02					1.79 (4–16)/59.07
TZ13	2.58 (17)/85.01	0.79 (5)/26.20					1.41 (9–16)/46.53
TZ13	2.45 (18)/70.00	0.86 (6)/28.50					0.72 (12–19)/23.76
TZ13	0.34 (19)/11.01	0.90 (7)/29.60					0.7 (12–20)/23.1
TZ13	0.89 (20)/29.21	3.48 (8)/114.90					
TZ13		0.90 (9)/29.60					
TZ13		3.48 (10)/114.90					
TZ13		3.04 (11)/100.30					
TZ13		3.32 (12)/109.9					

TMOpx: temperature calculation after [46] using orthopyroxene, TMCpx: using clinopyroxene, TW: temperature calculation after [47], TBK: temperature calculation after [48], TOW: temperature calculation after [49], TPCpx-Opx and PPCpx-Opx: temperature/pressure calculation after [50] using clinopyroxene and orthopyroxene, PMOpx and PMCpx: pressure calculation after [46] formula using clinopyroxene and orthopyroxene, GPa: gigapascal, n0: pyroxene, olivine and spinel analysis number as in Tables 4–6.

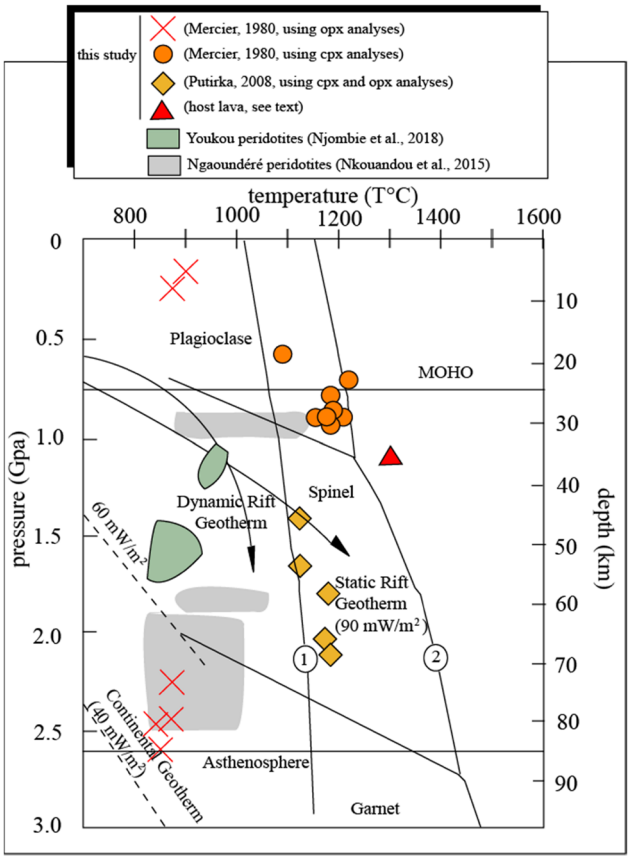

Figure 9: Equilibrium conditions of Hosséré Do Guessa wehrlites plotted in a temperature versus pressure (depth) diagram (adapted from [58]. Four values calculated between 3.04 and 3.48 GPa (Table 7) are not plotted in this diagram. Curves 1 and 2 are, respectively, the hydrous (0.4 wt% H_2O) and anhydrous solidi [78].

magma liquid [62,63]. However, many other features suggested by texture and mineral compositions show that Hosséré Do Guessa wehrlites are xenoliths from mantle origin. They are not consistent with the hypothesis of large volume of cumulates, since the latter are commonly associated with considerable compositional variation [64]. The poikilitic texture seems to be acquired during shallow mantle deformation which have led to strong recrystallisation of olivine [65]. As the northern part of Ngaoundéré basement have been transected in its large part by numerous Pan-African transpressive stick-slip-faults down to the mantle [13,22,28,29], reworking of these faults might have affected the shallow upper lithospheric mantle, as suggested by [42] for peridotite xenoliths of Iraya volcano in Japan.

Additionally, mineral composition of studied wehrlites strongly supports the mantle origin hypothesis of these rocks. Olivine is highly magnesian with Fo between 90.8 and 91.4 and has low CaO (<0.1 wt%, see [66]) and high NiO (0.24–0.48 wt%) contents, compatible with of mantle origin [67]. Cr# (Cr/Cr + Al) of spinel is low (12) and its composition plots in the mantle stability field of [41,68] with TiO_2 and Fe^{2+}/Fe^{3+} values close to mantle spinel composition. Clinopyroxene is Al-rich (5.0–5.9 wt% Al_2O_3) and orthopyroxene is Al-poor (0.7–1.3 wt% Al_2O_3, leading to inheritance from original garnet phase [69] after uplift [70].

Vertical movements under the Adamawa plateau have been suggested by geophysical studies [7]. The crust was uplifted by upward migration of the lithosphere-asthenosphere boundary from 180 to 80 km [2–6]. Poikilitic textures of Hosséré Do Guessa wehrlites may thus result from the solid-state tectonic relaxation as have been suggested by [34,71], consistent with the tectonic scenario. Hosséré Do Guessa wehrlites would not be comparable to cumulative wehrlites and xenoliths of magmatic origin from crystal mush, such as wehrlites described in Batoke, Mt. Cameroon volcano [31].

As the crustal thickness is estimated around 33–37 km at the north of Ngaoundéré, the studied xenoliths should have been sampled below, in the upper mantle, 50–66 km deep. The referring depths locate the wehrlite source close to the mantle-crust transition zone as that have been suggested by ref. [72]. It is thus possible that the wehrlite represents the uprising part of the high-temperature mantle peridotites, which have been metasomatized by magma fluids during upwelling (see below).

5.2 Melt-rock-fluid interactions: the wehrlite and carbonatite paradigm

Petrographic studies point out the presence of discrete orthopyroxene crystals and symplectite microtexture that are characteristic features of peridotites of mantle origin [73].

It is pointed out [74] that orthopyroxene-poor peridotites result, in general, from reactions with small volumes of carbonate/carbonatite melt, accompanying CO_2 degassing, according to the reaction: enstatite + dolomite (melt) → forsterite + diopside + CO_2 (vapour) ("wehrlitisation").

Fluids-rock interaction might have affected the lithospheric mantle beneath the Adamawa plateau as have been suggested [58]. Fluids might have circulated during or after tectonic recrystallization along Pan-African stick-slip-faults at high temperatures. The nature of the circulating fluids might be carbonatitic, as proposed by ref. [58] for Youkou sub-continental mantle. Pockets of

carbonate were identified in basalts, north and east of Ngaoundéré [61].

Later, re-equilibrations occurred at low depths (ca. 7 km) in the upper crust, following volcanic eruptions, with cooling from 900°C down to 750°C.

Numerous lukewarm (<22°C) springs are described north of Ngaoundéré [12]. Carbonated hot springs and geysers occur at 200–300 km north of Ngaoundéré, close to Tchabal Mbabo volcano.

6 Conclusion

Wehrlites from Hosséré Do Guessa volcano in Adamawa plateau have a mantle origin. They suffered movements of Pan-African strict-slip-faults during Adamawa upwelling at Tertiary times, after the solid state tectonic relaxation. Hosséré Do Guessa wehrlites result from reactions with carbonate/carbonatite melt, accompanying CO_2 degassing and then a metasomatic event after fluids phase circulation at depth. They have crystallized at 1.5–2.0 GPa, which corresponds to a depth of 50–66 km, at a temperature of 1,140–1,220°C, and then been equilibrated until 900–750°C, between 0.9 and 0.6 (perhaps until 0.2) GPa at shallow depth.

Acknowledgments: Authors greatly thank the "Agence Universitaire de la Francophonie (AUF)" through the BAGL (Bureau Afrique Centrale et des Grands Lacs), for financial support of "Le Projet de soutien aux équipes de recherche 2012/2013_No 51110SU201" in all aspect (from field works to laboratory analyses). The contribution of "Department of Earth Sciences, UMR CNRS 8148 GEOPS" of the University Paris-Saclay, France, is greatly appreciated. B. Bonin and A. Pouclet are warmly thanked for useful remarks. Fruitful remarks by F. Casetta and an anonymous reviewer have greatly helped us to improve the manuscript.

Author contributions: OFN, ZNNN, AFM and AH made field studies, JMB made electron microprobe analyses and OFN and JMB prepared the article.

Conflict of interest: Authors state no conflict of interest.

References

[1] Fagny AM, Nkouandou OF, Bardintzeff JM, Guillou H, Iancu GO, Ndassa ZNN, Temdjim R. Petrology and geochemistry of the Tchabal Mbabo volcano in Cameroon volcanic line (Cameroon, Central Africa): An intra-continental alkaline volcanism. J Afr Earth Sci. 2020;170(103832):1–27.

[2] Browne SE, Fairhead JD. Gravity study of the Central African Rift System: a model of continental disruption 1. The Ngaoundéré and Abu Gabra rifts. In: Morgan P, Baker BH, editors. Processes of planetary rifting. Tectonophysics. Vol. 94. 1983. p. 187–203.

[3] Girod M, Dautria JM, Ball E, Soba D. Estimation de la profondeur du Moho, sous le massif volcanique de l'Adamaoua (Cameroun), à partir de l'étude d'enclaves de lherzolite. Comptes Rendus de l'Académie des Sciences Paris 298 (II, 16); 1984. p. 699–704.

[4] Dautria JM, Girod M. Les enclaves de lherzolite à spinelle et plagioclase du volcan de Dibi (Adamaoua, Cameroun): des témoins du manteau anormal. Bull de Minéral. 1986;109:275–286.

[5] Fairhead JD, Okereke CS. Depths to major density contrast beneath the West-Africa rift system in Nigeria and Cameroon based on the spectral analysis of gravity of data. J Afr Earth Sci. 1988;7(5/6):769–77.

[6] Poudjom Djomani YH, Diament M, Albouy Y. Mechanical behavior of the lithosphere Beneath the Adamawa Up lift (Cameroon, West Africa) based on gravity data. J Afr Earth Sci. 1992;15:81–90.

[7] Poudjom Djomani YH, Diament M, Wilson M. Lithospheric structure across the Adamawa plateau (Cameroon) from gravity studies. Tectonophysics. 1997;237:317–27.

[8] Tokam APK, Tabod CT, Nyblade AA, Julià J, Wiens DA, Pasyanos ME. Structure of the crust beneath Cameroon, West Africa, from the joint inversion of Rayleigh wave group velocities and receiver functions. Geophys J Int. 2010;183(2):1061–76.

[9] De Plaen RSM, Bastow ID, Chambers EL, Keir D, Gallacher RJ, Keane J. The development of magmatism along the Cameroon Volcanic Line: Evidence from seismicity and seismic anisotropy. J Geophys Res Solid Earth. 2014;119(5):4233–52.

[10] Eyike A, Ebbing J. Lithospheric structure of the West and Central African Rift System from regional three-dimensional gravity modelling. South Afr J Geol. 2015;118(3):285–98.

[11] Ngalamo JFG, Bisso D, Abdelsalam MG, Atekwana EA, Katumwehe AB, Ekodeck GE. Geophysical imaging of meta-cratonizaton in the northern edge of the Congo craton in Cameroon. J Afr Earth Sci. 2017;129(94–107):2017.

[12] Njeudjang K, Abate Essi JM, Kana JD, Teikeu WA, Njandjock Nouck P, Djongyang N, et al. Gravity investigation of the Cameroon Volcanic Line in Adamawa region: Geothermal features and structural control. J Afr Earth Sci. 2020;165:103809.

[13] Dorbath C, Dorbath L, Fairhead JD, Stuart GW. A teleseismic delay time study across the central African Shear Zone in the Adamawa region of Cameroon. West Afr Geophys J R Astron Soc. 1986;86:751–66.

[14] Menzies MA, Halliday AN, Palacz Z, Hunter RH, Upton BGJ, Aspen P, et al. Evidence from mantle xenoliths for an enriched lithospheric keel under the Outer Hebrides. Nature. 1987;325:44–7.

[15] Lee DC, Halliday AN, Davies GR, Essene EJ, Fitton JG, Temdjim R. Melt enrichment of shallow depleted mantle: a detailed petrological, trace element and isotopic study of

mantle-derived xenoliths and megacrysts from the Cameroon Line. J Petrol. 1996;37:415–41.
[16] Temdjim R. Contribution à la connaissance du manteau supérieur du Cameroun au travers de l'étude des enclaves ultrabasiques et basiques remontées par les volcans de Youkou (Adamaoua) et de Nyos (Ligne du Cameroun). Thèse Doctorat d'Etat. Cameroun: Université Yaoundé1; 2005. p. 423
[17] Nkouandou OF, Temdjim R. Petrology of spinel lherzolite xenoliths and host basaltic lava from Ngao Voglar volcano, Adamawa Massif (Cameroon Volcanic Line, West Africa): equilibrium conditions and mantle characteristics. J Geosci. 2011;56:375–87.
[18] Nkouandou OF, Bardintzeff JM, Fagny AM. Sub-continental lithospheric mantle structure beneath the Adamawa plateau inferred from the petrology of ultramafic xenoliths from Ngaoundéré (Adamawa plateau, Cameroon, Central Africa). J Afr Earth Sci. 2015;111:26–40.
[19] Nnange JM, Ngako V, Fairhead JD, Ebinger CJ. Depths to density discontinuities beneath the Adamawa Plateau region, Central Africa, from spectral analyses of new and existing gravity data. J Afr Earth Sci. 2000;30(4):887–901.
[20] Tchameni R, Pouclet A, Penaye J, Ganwa AA, Toteu SF. Petrography and geochemistry of the Ngaoundéré Pan-African granitoids in central North Cameroon: implications for their sources and geological setting. J Afr Earth Sci. 2006;44:511–29.
[21] Ganwa AA, Frisch W, Siebel W, Ekodeck GE, Cosmas SK, Ngako V. Archean inheritances in the pyroxene-amphibole bearing gneiss of the Méiganga area (Central North Cameroon): Geochemical and 207Pb/206Pb age imprints. Comptes Rendus Géosc. 2008;340:211–22.
[22] Moreau C, Regnoult JM, Déruelle B, Bobineau B. A new tectonic model for Cameroon line, central Africa. Tectonophysics. 1987;139:317–34.
[23] Wilson M, Guiraud R. Magmatism and rifting in Western and Central Africa, from Late Jurassic to Recent times. Tectonophysics. 1992;213:203–25.
[24] Cornacchia M, Dars R. Un trait structural majeur du continent africain. Les linéaments centre africain du Cameroun au golfe d'Aden. Bull de la Soc Géolo de Fr. 1983;25:101–9.
[25] Guiraud R, Bosworth W, Thierry J, Delplanque A. Phanerozoic geological evolution of Northern and Central Africa: An overview. J Afr Earth Sci. 2005;43(1–3):83–143.
[26] Mbowou IBG, Nguihdama D, Yamgouot FN, Ntoumbe M, Youpoungam AA, Ngounouno I. Mineral chemistry of wehrlite xenoliths hosted in basalts from the SW of Hosséré Dammougalré (Adamawa Plateau, Cameroon): Thermobarometric implications. Open J Geol. 2017;7:1465–77.
[27] Pouchou JL, Pichoir F. Quantitative analysis of homogeneous or stratified microvolumes applying the model «PAP». In Electron Probe quantification. In: Heinriche DE. editor. Newbury, New York, US: Plenum Press; 1991. p. 31–75.
[28] Ngangom E. Étude tectonique du fossé Crétacé de la Mbéré et du Djérem, Sud Adamawa, Cameroun. Bull Cent de Rech Expl-Prod Elf-Aquitaine. 1983;7:339–47.
[29] Dumont JF. Étude structurale des bordures nord et sud du plateau de l'Adamaoua: influence du contexte atlantique. Géodynamique. 1987;2(1):56–68.
[30] Le Maitre RW, editor. Igneous rocks, a classification and glossary of terms. (Recommendations of the IUGS subcommission on the systematics of igneous rocks). Cambridge: Cambridge University Press; 2002. p. 252.
[31] Wandji P, Tsafack JPF, Bardintzeff JM, Nkouathio DG, Kagou Dongmo A, Bellon H, et al. Xenoliths of dunites, wehrlites and clinopyroxenites in the basanites from Batoke volcanic cone (Mount Cameroon, Central Africa): petrogenetic implications. Mineral Petrol. 2009;96(1):81–98.
[32] Shaw CSJ, Eyzaguirre J, Fryer B, Gagnon J. Regional variations in the mineralogy of metasomatic assemblages in mantle xenoliths from the West Eifel volcanic field, Germany. J Petrol. 2005;46(5):945–72.
[33] Villaseca C, Ancochea E, Orejana D, Jeffries TE. Composition and evolution of the lithospheric mantle in central Spain: inferences from peridotite xenoliths from the Cenozoic Calatrava volcanic field. In: Coltorti M, Downes H, Grégoire M, O'Reilly SY, editors. Petrological evolution of the European lithospheric mantle. Geological Society. 337, London: Special Publications; 2010. p. 125–51.
[34] Mercier JCC, Nicolas A. Textures and fabrics of upper-mantle peridotites as illustrated by xenoliths from basalts. J Petrol. 1975;16(2):454–87.
[35] Njankouo Ndassa ZN. 2019. Pétrologie et géochimie des péridotites en enclaves dans les basaltes de Ngaoundéré et ses environs: nature du manteau subcontinental sous le plateau de l'Adamaoua (Plateau de l'Adamaoua, Cameroun, Afrique centrale). Thèse Université de Ngaoundéré, 232 pp + annexes.
[36] Njankouo Ndassa ZN, Nkouandou OF, Bardintzeff JM, Ganwa AA, Fagny MA, Tizi A. Petrology of peridotite host basaltic lavas of northern Ngaoundéré (Adamawa plateau, Cameroon, Central Africa). Int J Adv Geosci. 2019;7(2):85–94.
[37] Wandji P, Bardintzeff JM, Ménard JJ, Tchoua FM. The alkaline fassaite-bearing volcanic province of the Noun Plain (West-Cameroon). Neues Jahrbuch für Mineralogie. Monatshefte. 2000;1:1–14.
[38] Embey-Isztin A. The role of melt depletion versus refertilization in the major element chemistry of four-phase spinel peridotite xenoliths. Central European. Geology. 2016;59(1–4):60–86.
[39] Rudnick RL, McDonough WF, Chappell BW. Carbonatite metasomatism in the northern Tanzanian mantle: petrographic and geochemical characteristics. Earth Planet Sci Lett. 1993;114:463–75.
[40] Morimoto N, Fabries J, Ferguson AK, Ginzburg IV, Ross M, Seifert FA, et al. Nomenclature of pyroxenes. Mineral Mag. 1988;52:535–50.
[41] Carswell DA. Mantle derived lherzolite nodules associated with kimberlite, carbonatite and basalt magmatism: A review. Lithos. 1980;13(2):121–38.
[42] Arai S. Characterization of spinel peridotites by olivine-spinel compositional relationships: review and interpretation. Chem Geol. 1994;113(3–4):191–204.
[43] Putirka KD, Perfit M, Ryerson FJ, Jackson MG. Ambient and excess mantle temperatures, olivine thermometry, and active vs. passive upwelling. Chem Geol. 2007;241(3–4):177–206.
[44] Putirka KD, Mikaelian H, Ryerson FJ, Shaw H. New clinopyroxene-liquid thermobarometers for mafic, evolved, and volatile-bearing lava compositions, with applications to lavas from Tibet and the Snake River Plain, Idaho. Am Mineral. 2003;88(10):1542–54.

[45] Lindsley DH. Pyroxene thermometry. Am Mineral. 1983;68(5–6):477–93.
[46] Mercier JCC. Single-pyroxene thermobarometry. Tectonophysics. 1980;70:1–37.
[47] Wells PRA. Pyroxene thermometry in simple and complex systems. Contrib Mineral Petrol. 1977;62:129–39.
[48] Brey GP, Köhler T. Geothermobarometry in four phase lherzolites II. New thermobarometers, and practical assessment of existing thermometers. J Petrol. 1990;31:1353–78.
[49] O'Neill HStC, Wall VJ. The olivine–orthopyroxene–spinel oxygen geobarometer, the nickel precipitation curve, and the oxygen fugacity of the Earth's upper mantle. J Petrol. 1987;28:1169–91.
[50] Putirka KD. Thermometers and barometers for volcanic systems. Rev Mineral Geochem. 2008;69(1):61–120.
[51] Glaser SM, Foley SF, Günther D. Trace element compositions of minerals in garnet and spinel peridotite xenoliths from the Vitim volcanic field, Transbaikalia, eastern Siberia. Lithos. 1999;48(1–4):263–85.
[52] Medaris Jr,GL, Wang HF, Fournelle JH, Zimmer JH, Jelínek E. A cautionary tale of spinel peridotite thermobarometry: an example from xenoliths of Kozákov volcano. Czech Repub Geolines. 1999;9:92–6.
[53] Köhler TP, Brey GP. Calcium exchange between olivine and clinopyroxene calibrated as a geothermobarometer for natural peridotites from 2 to 60 kb with applications. Geochim Cosmochim Acta. 1990;54:2375–88.
[54] O'Reilly SY, Chen D, Griffin WL, Ryan CG. Minor elements in olivine from spinel lherzolite xenoliths: implications for thermobarometry. Mineral Mag. 1997;61:257–69.
[55] Christensen NI, Medaris JrLG, Wang HF, Jelinek E. Depth variation of seismic anisotropy and petrology in central European lithosphere: a tectonothermal synthesis from spinel lherzolites. J Geophys Res. 2001;160(B1):645–64.
[56] Nimis P. Clinopyroxenes from plagioclase peridotites (Zabargad Island, Red Sea) and comparison between high- and low-pressure mantle clinopyroxenes. Mineral Petrol. 1995;53(1–3):49–61.
[57] O'Neill HStC. The transition between spinel lherzolite and garnet lherzolite, and its use as a geobarometer. Contrib Mineral Petrol. 1981;77(2):185–94.
[58] Njombie MPW, Temdjim R, Foley SF. Petrology of spinel lherzolite xenoliths from Youkou volcano, Adamawa Massif, Cameroon Volcanic Line: mineralogical and geochemical fingerprints of sub-rift mantle processes. Contrib Mineral Petrol. 2018;173:173–193.
[59] Meshesha D, Shinjo R, Orihashi Y. Geochemical and Sr-Nd-Pb isotopic compositions of lithospheric mantle: Spinel lherzolites in alkaline basalts from the northwestern Ethiopian plateau. J Mineral Petrol Sci. 2014;109(6):241–57.
[60] Nkouandou OF, Ngounouno I, Déruelle B, Ohnenstetter D, Montigny R, Demaiffe D. Petrology of the Mio-Pliocene Volcanism to the North and East of Ngaoundéré (Adamawa-Cameroon). Comptes Rendus Géosci. 2008;340:27–38.
[61] Nkouandou OF, Ngounouno I, Déruelle B. Géochimie des laves basaltiques récentes des zones Nord et Est de Ngaoundéré (Plateau de l'Adamaoua, Cameroun, Afrique Centrale): pétrogenèse et nature de la source. Int J Biol Chem Sci. 2010;4(4):984–1003.
[62] Lippard SJ, Shelton AW, Gass LG. ophiolite North Oman Mem Geol Soc Lond. 1986;11:178.
[63] Girardeau J, Francheteau J. Plagioclase-wehrlites and peridotites on the East Pacific Rise (Hess Deep) and the Mid-Atlantic Ridge (DSDP Site 334): Evidence for magma percolation in the oceanic upper mantle. Earth Planet Sci Lett. 1993;115:137–49.
[64] Xu YG, Menzies MA, Bodinier J-L, Bedini RM, Vroon P, Mercier JCC. Melt percolation and reaction atop a plume: evidence from the poikiloblastic peridotite xenoliths from Borée (Massif Central, France). Contrib Mineral Petrol. 1998;132(1):65–84.
[65] Kaczmarek MA, Bodinier JL, Bosch D, Tommasi A, Dautria JM, Kechid SA. Metasomatized Mantle Xenoliths as a Record of the Lithospheric Mantle Evolution of the Northern Edge of the Ahaggar Swell, In Teria (Algeria). J Petrol. 2016;57(2):345–82.
[66] Simkin T, Smith JV. Minor-element distribution in olivine. J Geol. 1970;78(3):304–25.
[67] Roeder PL, Emslie RF. Olivine-liquid equilibrium. Contrib Mineral Petrol. 1970;29:275–89.
[68] Lenaz D, Kamenetsky VS, Crawford AJ, Princivalle F. Melt inclusions in detrital spinels from the SE Alps (Italy–Slovenia): a new approach to provenance studies of sedimentary basins. Contrib Mineral Petrol. 2000;139:748–58.
[69] Dawson JB, Smith JV. Upper-mantle amphiboles: a review. Mineral Mag. 1982;45:35–46.
[70] Wallace ME, Green DH. The Effect of Bulk Rock Composition on the Stability of Amphibole in the upper Mantle: Implications for solidus positions and mantle metasomatism. Mineral Petrol. 1991;44:1–19.
[71] Mercier JCC. Natural peridotites: chemical and rheological heterogeneity of the upper mantle. USA: PhD, University of New York Stony Brook; 1976.
[72] Benn K, Nicolas A, Reuber I. Mantle-crust transition zone and origin of wehrlitic magmas: Evidence from the Oman ophiolite. Tectonophysics. 1988;151:75–85.
[73] Chen CH, Presnall DC, Stern RJ. Petrogenesis of Ultramafic Xenoliths from the 1800 Kaupulehu Flow, Hualalai Volcano, Hawaii. J Petrol. 1992;33:163–202.
[74] Aulbach S, Lin A-B, Weiss Y, Yaxley GM. Wehrlites from continental mantle monitor the passage and degassing of carbonated melts. Geochem Perspect Lett. 2020;15:30–4.
[75] Temdjim R. Ultramafic xenoliths from Lake Nyos area, Cameroon volcanic line, West-central Africa: Petrography, mineral chemistry, equilibration conditions and metasomatic features. Geochemistry - Chemie der. Erde. 2012;72(1):39–60.
[76] Caldeira R, Munhá JM. Petrology of ultramafic nodules from São Tomé Island, Cameroon Volcanic Line (oceanic sector). J Afr Earth Sci. 2002;34(3–4):231–46.
[77] Rocco I, Lustrino M, Zanetti A, Morra V, Melluso L. Petrology of ultramafic xenoliths in Cenozoic alkaline rocks of northern Madagascar (Nosy Be Archipelago). J South Am Earth Sci. 2013;41:122–39.
[78] Falloon TJ, Green DH, O'Neill HS, Hibberson WO. Experimental tests of low degree peridotite partial melt compositions: implications for the nature of anhydrous near-solidus peridotite melts at 1 GPa. Earth Planet Sci Lett. 1997;152(1–4):149–62.